J. Fluid Mech. (2009), *vol.* 623, *pp.* 317–327.
doi:10.1017/S0022112008005144 Printed in the United Kingdom

Characterising line fountains

G. R. HUNT† AND C. J. COFFEY

Department of Civil and Environmental Engineering, Imperial College London, London, SW7 2AZ, UK

(Received 4 August 2008 and in revised form 23 October 2008)

We present analytical solutions for the initial rise height z_m of two-dimensional turbulent fountains issuing from a horizontal linear source of width $2b_0$ into a quiescent environment of uniform density. Using the initial rise height prediction as a measure we classify line fountains into three types depending on their source conditions. For source Froude numbers $Fr_0 \gg 1$, the near-source flow of the 'forced' fountain is dominated by source momentum flux and behaves like a jet; the asymptotic solution to the fountain equations yields, in agreement with previous studies, $z_m/b_0 \sim Fr_0^{4/3}$. For $Fr_0 = O(1)$ the fountain is 'weak' and fluid is projected vertically to a height that is consistent with an energy-conserving flow – the sensitivity of the rise height with Fr_0 increases as $z_m/b_0 \sim Fr_0^2$. For $Fr_0 \ll 1$, the fountain is 'very weak' and we find that $z_m/b_0 \sim Fr_0^{2/3}$. As the local value of the Froude number decreases with height, all three forms of fountain behaviour identified are expected above a highly forced source and we provide scalings for the three lengths that contribute to the total rise height. Comparisons between our predicted rise heights and the previous experimental results show good agreement across a wide range of Fr_0. The collated data highlights that experiments have focused in the majority on fountains above sources with intermediate Fr_0. Notably there is a lack of measurements on very weak line fountains and of independent experimental confirmation of the initial rise heights across the range of Fr_0.

1. Introduction

The question of determining the rise height of turbulent fountains, that is the continuous vertically-forced supply of negatively buoyant fluid upwards from a localized source into a less-dense quiescent unbounded environment, was raised and examined by Turner (1966). Campbell & Turner (1989) and Baines, Turner & Campbell (1990) expanded Turner's investigations of circular sources to consider releases from a long horizontal line source. The resulting line fountain is assumed to be two-dimensional as variations in the longitudinal direction are typically weak. Fluid is projected upwards due to the source momentum flux. The momentum flux is reduced locally in the rising fluid by the action of the opposing buoyancy force until the fluid reverses direction and falls back towards the source. This downflow retards subsequent upflowing fluid, resulting in the rise height decreasing from the initial maximum. Figure 1 shows a schematic illustration of a line fountain.

Line fountains occur, or are generated, across a range of physical scenarios and engineering applications. For example, air curtains (Guyonnaud *et al.* 2000) created

† Email address for correspondence: gary.hunt@ic.ac.uk

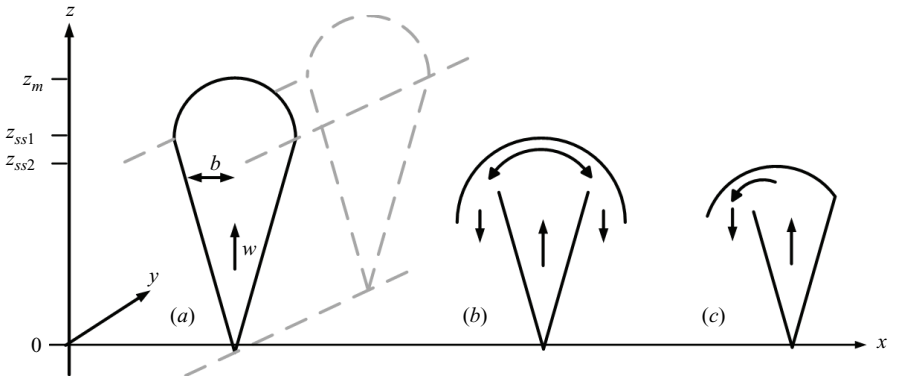

FIGURE 1. Schematic illustration of a line fountain. (*a*) The fountain head initially rises to a maximum height (z_m) before settling back and intermittently switching between two 'steady' heights; (*b*) z_{ss1} and (*c*) z_{ss2}. The notation '*m*', '*ss*1' and '*ss*2' is used to distinguish between rise heights.

by injecting warm air downwards are commonly used in tunnels and shop entrances as a means of segregating regions of fluid. A row of closely spaced axisymmetric fountains may be approximated as a line fountain (Baines *et al.* 1990) as, for example, in underfloor air distribution systems where the aim is to provide replacement cool air from horizontal vents at floor level (Liu & Linden 2006). A consequence of a thermal or fire plume (Cooper 1988) in a room is the projection of buoyant fluid downwards, as a line fountain, when the ceiling current impinges on the sidewall – the characteristics and subsequent penetration of this fountain depending on the room aspect ratio (Kaye & Hunt 2007).

Baines *et al.* (1990) presented experimental results describing 'forced' line fountains, that is fountains with a large momentum flux at the source relative to the source buoyancy flux. They showed that a symmetrical downflow with fluid moving equally down each side of the upflowing region is not generally maintained (figure 1). Instead, the fountain head is unstable and fluctuates between the extremes of a symmetrical downflow and an asymmetrical downflow in which the downflowing fluid is confined to one side of the line source. During periods of asymmetrical downflow a significant decrease in the fountain height was observed. Baines *et al.* (1990) noted that the flow appeared to switch randomly between the two states and as such no time scale for the cycle could be ascertained.

Measurements of the initial (maximum) height of the forced line fountain (z_m) were shown to scale on the source momentum jet length ($L_M(z=0) \equiv L_{M0}$), i.e.

$$z_m \sim L_{M0} \sim M_0 F_0^{-2/3}, \tag{1.1}$$

where M_0 and F_0 are the source momentum flux per unit length and buoyancy flux per unit length, respectively. Assuming a uniform velocity profile at the source (1.1) can be written in terms of a source Froude number ($Fr_0 = w_0/\sqrt{b_0 g_0'}$) as

$$\frac{z_m}{b_0} \sim Fr_0^{4/3} = 2^{2/3}\left(\frac{M_0^3}{Q_0^3 F_0}\right)^{2/3}, \tag{1.2}$$

where Q_0 is the source volume flux per unit length and w_0, b_0 and $g_0' = g(\rho_0 - \rho_a)/\rho_a$ are the source vertical velocity, half-width and reduced gravity, respectively. The densities ρ_0 and ρ_a are those of the source and ambient, respectively. Based on an

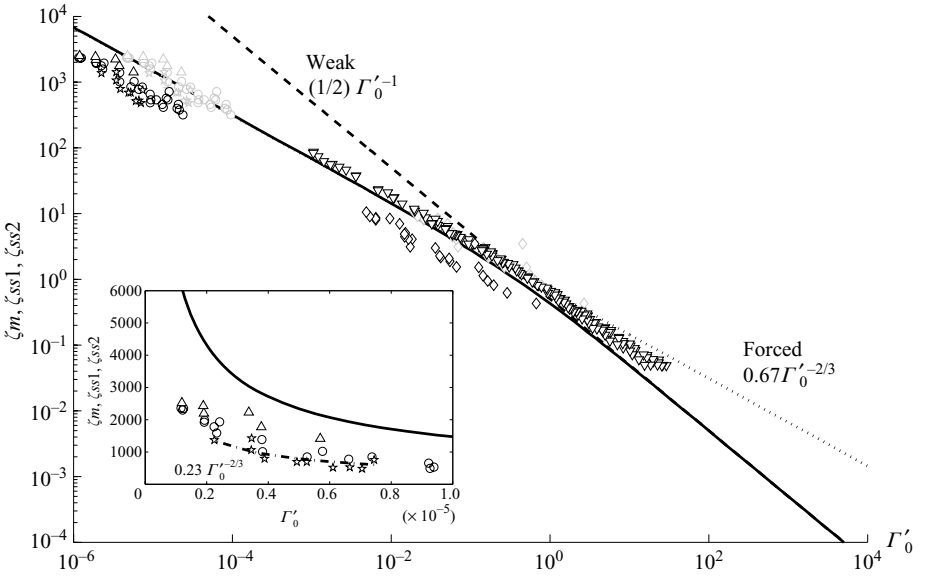

FIGURE 2. The rise height ζ_m as a function of Γ_0' from (2.8). The numerical solution of (2.8) (solid line) is shown together with the forced fountain asymptotic solution (2.13) (dotted line) and the weak fountain asymptotic solution (2.16) (dashed line). Also plotted are the experimental data of Campbell & Turner (1989, ◇ , *ss*1), Baines *et al.* (1990, △, *m*; ○, *ss*1 and ☆, *ss*2) and Zhang & Baddour (1997, ▽, *m*). The faint grey symbols show the shift in the Baines *et al.* (1990) data achieved by doubling their Fr_0 (cf. (1.4)). The inset figure is an enlargement of the small Γ_0' region (with linear axes), the dash-dot line $\zeta_{ss2} = 0.23\Gamma_0'^{-2/3}$ is a least-squares fit to ☆.

empirical fit to their data, Baines *et al.* (1990) gave

$$\frac{z_m}{b_0} = 0.65 Fr_0^{4/3} \quad \text{for} \quad 5 \lesssim Fr_0 \lesssim 1000. \tag{1.3}$$

We have been made aware (Kerr & Turner 2008) that an error (resolved by replacing Fr_0 with $2Fr_0$) may exist in the scaling and presentation of data by Baines *et al.* (1990), and that the true scaling (cf. (1.3)) should read

$$\frac{z_m}{b_0} = 0.65(2Fr_0)^{4/3} \approx 1.64 Fr_0^{4/3}. \tag{1.4}$$

This result is consistent with the rise heights obtained by Bloomfield & Kerr (1998) for an unstratified environment using the same experimental rig as used by Baines *et al.* (1990). Whilst this supports the possibility of an error and brings the results of Baines *et al.* (1990) in line with other measurements it is not possible to substantiate the error directly from their published work. The data as recorded by Baines *et al.* (1990) and on accounting for the error are shown in figure 2.

Zhang & Baddour (1997) also measured the rise heights of line fountains but for weaker fountains towards the lower end of the Froude number range considered by Baines *et al.* (1990). Zhang & Baddour (1997) generated fountains by forcing fluid through slots of varying aspect ratios. Their experimental data supported the 4/3-power law, with

$$\frac{z_m}{b_0} = 2.0 Fr_0^{4/3} \quad \text{for} \quad 6.5 \lesssim Fr_0 \lesssim 113, \tag{1.5}$$

i.e. rise heights over three times those of Baines *et al.* (1990) based on (1.3), or closer to 20 % based on (1.4). The differences in the source geometry used by these authors may account for part of this variation. By generating fountains using a row of closely spaced circular holes, the near-source axisymmetric flows of the Baines *et al.* (1990) fountains would be expected to have greater entrainment and thus lead to a lower rise height than for a fountain from an actual line source such as a slot. The disparity between the rise heights of Baines *et al.* (1990) and Zhang & Baddour (1997), both measured by eye and from nozzles of similar scales, highlights the sensitivity of fountain behaviour to the method of generation. Of note is the lack of independent corroboration of fountain rise height measurements and limited overlap between the various authors' range of measurements (see figure 2).

For even smaller values of the source Froude number, Zhang & Baddour (1997) argued that an alternative scaling was required as the buoyancy flux dominates in the near-source flow of these 'weaker' fountains. They presented two models. In the first, they assumed the fountain was equivalent to that which develops from a virtual source of momentum flux M_0 and buoyancy flux F_0 only. Dimensional arguments suggest the distance z_v between the virtual and real sources scales as $z_v/b_0 \propto Fr_0^{2/3}$ and, based on an empirical fit,

$$\frac{z_m}{b_0} = 2.0Fr_0^{4/3} - \frac{z_v}{b_0} = \left(2.0 - 1.12Fr_0^{-2/3}\right)Fr_0^{4/3} \quad \text{for} \quad 0.62 \lesssim Fr_0 \lesssim 6.5. \tag{1.6}$$

This reduces to (1.5) for large Fr_0. The origin correction reduces the fountain rise height significantly across the range of Fr_0 considered, though not enough to account for the discrepancy between (1.3) and (1.5). Zhang & Baddour (1997) also discussed an alternative scaling based on the time for the fountain to reach the maximum rise height $t_m \sim M_0/F_0$. Taking the characteristic vertical velocity as w_0, they argued that $z_m \propto w_0 t_m \propto (M_0/Q_0)(M_0/F_0) \propto b_0 Fr_0^2$, and a fit to their experimental data gave

$$\frac{z_m}{b_0} = 0.71Fr_0^2 \quad \text{for} \quad 0.62 \lesssim Fr_0 \lesssim 6.5. \tag{1.7}$$

Lin & Armfield (2000) also consider 'weak' line fountains. Their dimensional considerations for $Fr_0 = O(1)$ and small values of the source Reynolds number $Re_0 = w_0 b_0/\nu$, where ν is the kinematic viscosity, led to $z_m/b_0 \sim Fr_0/\sqrt{Re_0}$, whereas for sufficiently large values of the source Reynolds number

$$\frac{z_m}{b_0} \sim Fr_0^{4/3}, \tag{1.8}$$

i.e. the same power-law dependence as (1.2).

For very weak fountains, i.e. $Fr_0 \ll 1$, the effect of viscosity was deemed important and Lin & Armfield (2000) determined that, in this regime, the rise height scalings are the same as for the axisymmetric fountain with $z_m/b_0 \sim (Fr_0/Re_0)^{2/3}$. Numerical simulation suggested that at $Re_0 = 200$

$$\frac{z_m}{b_0} \approx 1.88Fr_0^{2/3}. \tag{1.9}$$

There is clearly some discrepancy in the literature regarding the rise height of line fountains and in the ranges of source Froude numbers for which the resulting fountains may be regarded as 'forced', 'weak' or 'very weak'. To an extent this has been compounded by the challenges in experimentally producing line fountains with constant and uniform conditions per unit length, and of consistently measuring the rise height of the inherently unstable fountain head.

Herein, we consider turbulent line fountains across the entire range of Fr_0. Our objective is to classify line fountains based on the relative magnitudes of the source fluxes and the corresponding rise height scalings. Following Kaye & Hunt (2006) we recast in § 2 the conservation equations of Morton, Taylor & Turner (1956) for line fountains in terms of a Richardson number (Γ) and a dimensionless fountain width (β). Their asymptotic solutions reveal the scalings for the rise heights and these are validated by comparisons with existing experimental and numerical data. We then consider the transitional behaviour with height within a fountain from a highly forced source. In § 3 we present our conclusions.

2. Analytical solutions for the initial rise height

Assuming Gaussian profiles for the vertical velocity $w(z, x) = w_m e^{-x^2/b^2}$ and reduced gravity $g'(z, x) = g'_m e^{-x^2/b^2}$, the conservation equations for a constant buoyancy flux plume from a horizontal line source at $z = 0$ in a quiescent uniform environment may be written in terms of the fluxes per unit length of volume ($Q_l = \pi^{1/2} b w_m$), momentum ($M_l = (\pi/2)^{1/2} b w_m^2$) and buoyancy ($F_l = (\pi/2)^{1/2} b g'_m w_m$) as (Hunt & Kaye 2001)

$$\frac{\mathrm{d}Q_l}{\mathrm{d}z} = 2^{3/2}\alpha\frac{M_l}{Q_l}, \qquad \frac{\mathrm{d}M_l}{\mathrm{d}z} = \frac{Q_l F_l}{M_l}, \qquad \frac{\mathrm{d}F_l}{\mathrm{d}z} = 0, \tag{2.1}$$

where b is the fountain half-width (taken as the value of x at which the velocity is 1/e of its centreline value w_m) and α is the entrainment coefficient.

The conservation equations (2.1) may be expressed in terms of a Richardson number Γ_l describing the relative magnitudes of the fluxes Q_l, M_l and F_l at a height z (Hunt & Kaye 2001; Kaye & Hunt 2006) and a dimensionless width β of the plume:

$$\Gamma_l = 2^{-3/2}\alpha_{jet}^{-1}\frac{Q_l^3 F_l}{M_l^3} = 2^{-1/2}\alpha_{jet}^{-1} Fr_l^{-2}, \qquad \beta = \frac{Q_l^2}{M_l}\frac{M_0}{Q_0^2} = \frac{b}{b_0}. \tag{2.2}$$

Here α_{jet} (≈ 0.0515, see, for example, Kotsovinos & List 1977) denotes the entrainment coefficient for a line jet. In terms of Γ_l and β the conservation equations (2.1) become

$$\frac{\mathrm{d}\Gamma_l}{\mathrm{d}\zeta} = 3\frac{\Gamma_l}{\beta}(\phi - \Gamma_l), \qquad \frac{\mathrm{d}\beta}{\mathrm{d}\zeta} = 2\phi - \Gamma_l, \tag{2.3}$$

where the vertical coordinate is scaled on the source width such that $\zeta = 2^{3/2}\alpha_{jet} M_0 Q_0^{-2} z = 2^{1/2}\alpha_{jet}(z/b_0)$. The parameter $\phi = \alpha/\alpha_{jet}$ introduced as the entrainment coefficient for line fountains is not well understood and is unlikely to be independent of height, however, we expect $\phi = O(1)$.

The source Richardson number for fountains $\Gamma_0 \equiv \Gamma_l(\zeta = 0) < 0$, as $F_0/M_0 < 0$, and for convenience we introduce $\Gamma'_l = -\Gamma_l > 0$. The governing equations (2.3) are then

$$\frac{\mathrm{d}\Gamma'_l}{\mathrm{d}\zeta} = 3\frac{\Gamma'_l}{\beta}(\phi + \Gamma'_l), \qquad \frac{\mathrm{d}\beta}{\mathrm{d}\zeta} = 2\phi + \Gamma'_l, \tag{2.4}$$

and the fountain source conditions $Q_l = Q_0$, $M_l = M_0$ and $F_l = F_0$ at $z = 0$ reduce to

$$\Gamma'_l = \Gamma'_0, \quad \beta = 1 \quad \text{at} \quad \zeta = 0. \tag{2.5}$$

Solving (2.4) subject to (2.5) yields β in terms of Γ'_l,

$$\beta = \left(\frac{\Gamma'_l}{\Gamma'_0}\right)^{2/3}\left(\frac{\phi + \Gamma'_0}{\phi + \Gamma'_l}\right)^{1/3}. \tag{2.6}$$

Substituting (2.6) into (2.4) yields the variation of Γ_l' with height so that

$$\frac{\mathrm{d}\Gamma_l'}{\mathrm{d}\zeta} = 3\frac{\Gamma_0'^{2/3}}{(\phi+\Gamma_0')^{1/3}}\Gamma_l'^{1/3}(\phi+\Gamma_l')^{4/3}. \tag{2.7}$$

We expect the fountain to reach its initial maximum height ζ_m when $\Gamma_l' \to \infty$ (and $\beta \to \infty$, see (2.6)), thus

$$\zeta_m = \frac{1}{3}\frac{(\phi+\Gamma_0')^{1/3}}{\Gamma_0'^{2/3}}\int_{\Gamma_0'}^{\infty} \Gamma_l'^{-1/3}(\phi+\Gamma_l')^{-4/3}\,\mathrm{d}\Gamma_l'. \tag{2.8}$$

Figure 2 shows the numerical solution of (2.8) with $\phi = 1$ obtained using an adaptive Simpson quadrature. Expanding the integrand in (2.8) we obtain the following small and large Γ_l' limits which are used in §§2.1 and 2.2:

$$\Gamma_l'^{-1/3}(\phi+\Gamma_l')^{-4/3} = \begin{cases} \Gamma_l'^{-1/3}\phi^{-4/3} + O_{\Gamma_l'\to 0}\left(\Gamma_l'^{2/3}\right) \\ \Gamma_l'^{-5/3} + O_{\Gamma_l'\to\infty}\left(\Gamma_l'^{-8/3}\right) \end{cases}. \tag{2.9}$$

2.1. *Highly forced fountains* ($\Gamma_0' \ll 1$)

For small values of Γ_l' the fountain is highly forced and behaves like a jet. It is therefore reasonable to make (in (2.8)) the approximation $\phi + \Gamma_l' \approx \phi \approx 1$ as $\alpha \approx \alpha_{jet}$. The error associated with this approximation as $\Gamma_l' \to 0$ is given in (2.9). The value of Γ_l' increases with ζ, thus, this approximation will not be valid over the entire rise height and will fail once $\Gamma_l' \geqslant \Gamma_{lim}'$, where Γ_{lim}' denotes some limiting value of Γ_l'. Using approximation (2.9) for the near-field region allows the initial rise height ζ_m (2.8) to be expressed as

$$\zeta_m \approx \frac{1}{3}\frac{1}{\Gamma_0'^{2/3}}\left(\int_{\Gamma_0'}^{\Gamma_{lim}'} \Gamma_l'^{-1/3}\,\mathrm{d}\Gamma_l' + I\right) \quad \text{where} \quad I = \phi^{1/3}\int_{\Gamma_{lim}'}^{\infty} \Gamma_l'^{-1/3}(\phi+\Gamma_l')^{-4/3}\,\mathrm{d}\Gamma_l'. \tag{2.10}$$

Evaluating the first integral yields

$$\zeta_m \approx \frac{1}{2\Gamma_0'^{2/3}}\left[\Gamma_{lim}'^{\,2/3} - \Gamma_0'^{2/3} + \frac{2I}{3}\right]. \tag{2.11}$$

As $\Gamma_{lim}'/\Gamma_0' \gg 1$,

$$\zeta_m \approx \frac{1}{2}\left[\Gamma_{lim}'^{\,2/3} + \frac{2I}{3}\right]\Gamma_0'^{-2/3} \propto \Gamma_0'^{-2/3} \tag{2.12}$$

and a fit to the full numerical solution of (2.8) gives

$$\zeta_m \approx 0.67\Gamma_0'^{-2/3} \quad \text{for} \quad \Gamma_0' \ll 1. \tag{2.13}$$

Figure 2 shows the asymptotic solution (2.13) for the initial rise height (ζ_m) plotted with the experimental data of Campbell & Turner (1989, $\diamond$, *ss*1), Baines *et al.* (1990, $\triangle$, *m*), both extracted from figure 14 in Baines *et al.* (1990) and Zhang & Baddour (1997, $\triangledown$, *m*). Equation (2.13) may be expressed in terms of the source Froude number as

$$\frac{z_m}{b_0} \approx 0.60\alpha_{jet}^{-1/3}Fr_0^{4/3} \approx 1.61Fr_0^{4/3} \tag{2.14}$$

which lies between (1.3) and (1.5). In fact (1.3) was calculated by Baines *et al.* (1990) based on a fit to data that included measurements of the two steady-state rise heights ζ_{ss1} and ζ_{ss2} (shown as $\circ$ and $\star$, respectively, in figure 2). As ζ_{ss1} and ζ_{ss2} are typically

less than ζ_m the inclusion of this data will lead to a reduction in the constant of proportionality. Restricting the fit to the data solely on the *initial* rise height gives

$$\frac{z_m}{b_0} \approx 0.84 Fr_0^{4/3} \tag{2.15}$$

– marginally improved in comparison to Zhang & Baddour's result (1.5) and to our asymptotic solution (2.14).

We expect the steady rise heights ζ_{ss1} and ζ_{ss2} to follow the same scalings as ζ_m, i.e. for $\{\zeta_{ss1}, \zeta_{ss2}\} \sim \Gamma_0'^{-2/3}$. The asymmetric case ζ_{ss2} provides the lower bound to the line fountain's possible rise height, thus fitting the available data (see the dash-dot line in figure 2, inset) we expect the steady-state rise height of a forced line fountain ζ_{ss} to be bounded by $0.23\Gamma_0'^{-2/3} \approx \zeta_{ss2} \lesssim \zeta_{ss} \lesssim \zeta_m \approx 0.67\Gamma_0'^{-2/3}$.

2.2. *Weak fountains* ($\Gamma_0' \gtrsim 1$)

For weak line fountains $\Gamma_l' \gg \phi$ and we may reasonably assume $\phi + \Gamma_l' \approx \Gamma_l'$ (see (2.9)). From (2.8) the initial rise height ζ_m is thus approximated using (2.9) by

$$\zeta_m \approx \frac{1}{3}\Gamma_0'^{-1/3} \int_{\Gamma_0'}^{\infty} \Gamma_l'^{-5/3}\, \mathrm{d}\Gamma_l' = \frac{1}{2}\Gamma_0'^{-1}. \tag{2.16}$$

This is the same scaling as derived by Kaye & Hunt (2006) for axisymmetric fountains and implies the initial rise height for weak fountains is independent of the entrainment coefficient and scales on the square of the source Froude number. As with the axisymmetric case, this scaling gives $z_m \sim w_0^2/g_0'$ suggesting that the source kinetic energy is completely converted to potential energy and thus, energy is conserved.

Figure 2 shows the weak fountain asymptotic solution together with the full numerical solution of (2.8). Based on our classifications, the majority of the data on line fountain rise heights falls into a region of intermediate source Froude number where the rise height behaviour is between $\zeta_m \sim \Gamma_0'^{-2/3}$ and $\zeta_m \sim \Gamma_0'^{-1}$ asymptotes. The relative error $\varepsilon = (\mathrm{d}\Gamma_l'/\mathrm{d}\zeta)_{approx}/(\mathrm{d}\Gamma_l'/\mathrm{d}\zeta)_{exact}|_{\Gamma_l'=\Gamma_0'}$ associated with our small and large Γ_0' approximations can be used to estimate the value of Γ_0' for which the flow will move from forced to weak behaviour on increasing Γ_0' (or indeed Γ_l'). We assume that this transition occurs when relative errors are equal for both approximations. From the asymptotic approximations for forced and weak cases (see §§ 2.1 and 2.2, respectively), $\varepsilon_{forced} = \varepsilon_{weak}$ requires $(\phi + \Gamma_0')^{-1} = \Gamma_0'(\phi + \Gamma_0')^{-1}$ and, thus, this transition occurs for $\Gamma_0' = 1$. Whilst this forced-weak transition is based on the source value Γ_0', we note that for a forced fountain source, this transition will occur at the height at which $\Gamma_l'(\zeta) \approx 1$ is attained.

2.3. *Very weak fountains* ($\Gamma_0' \to \infty$)

For very large values of Γ_l' the width of the fountain may become large compared to its vertical extent and the validity of the assumptions implicit in the plume equations becomes questionable. The numerical data of Lin & Armfield (2000) suggest a different scaling (1.9) may apply in this limit.

The very weak fountain limit we considered is indicated schematically in figure 3. Fluid ejected vertically from the source with low momentum flux spills over the nozzle with the rise height z_{ss} providing the pressure head and driving critical flow at $x = b_0$. No entrainment is expected and hence the velocity of the outflow may be expressed as $u_{out} = c_d\sqrt{z_c g_0'}$, where $0 < c_d \leqslant 1$ is a dimensionless coefficient accounting for energy losses due, for example, to the surface roughness and nozzle geometry (e.g. whether a raised nozzle, figure 3*a*, or a flush nozzle, figure 3*b*). Conservation of volume

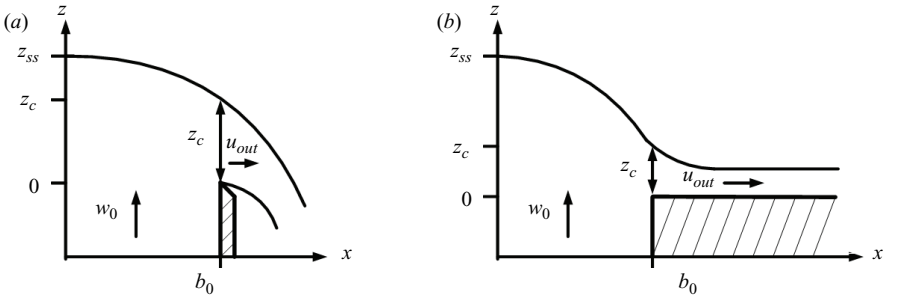

FIGURE 3. Schematics of a very weak line fountain. (*a*) Raised nozzle. (*b*) Flush nozzle.

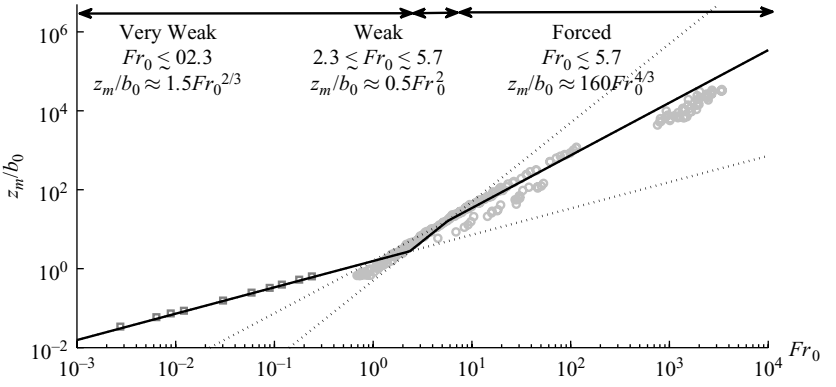

FIGURE 4. z_m/b_0 vs Fr_0 encompassing forced, weak and very weak source conditions. The circles show the existing experimental data of figure 2. The squares show the numerical data of Lin & Armfield (2000). The upper limit $Fr_0 \approx 5.7$ of the weak regime is included for illustrative purposes and is the value at which weak and forced asymptotes intersect.

requires

$$Q_0 = 2b_0w_0 = 2z_cu_{out} = 2c_dg_0'^{1/2}z_c^{3/2}. \tag{2.17}$$

Applying Bernoulli's theorem along the streamline marking the interface between the fountain fluid and ambient, from $x = 0$ to $x = b_0$, yields $z_c = (2/3)z_{ss}$ (see, for example, White 2003). Rearranging (2.17) and substituting for z_c yields

$$\frac{z_{ss}}{b_0} = \frac{3}{2}\frac{1}{c_d^{2/3}}Fr_0^{2/3}. \tag{2.18}$$

This analysis is analogous to that applied when modelling flow over a two-dimensional weir (Batchelor 1967). Equation (2.18) leads to the initially counterintuitive result that a decrease in c_d (i.e. an increase in energy loss) results in an increase in the fountain height. However, this must be the case as a volume flux b_0w_0 at $x = b_0$ can only be maintained as energy losses increase by raising the pressure head and hence the height of the fountain.

Taking $c_d = 1$, we have $z_{ss}/b_0 = 1.5Fr_0^{2/3}$ (cf. Lin & Armfield 2000), (1.9). To obtain their constant value of 1.88 would require $c_d = 0.45$. Figure 4 plots (2.18) together with the numerical data of Lin & Armfield (2000, □, *ss*1), showing a good comparison. The transition from weak to very weak is shown graphically to occur at $Fr_0 \approx 2.3$ ($\Gamma_0' \approx 2.6$).

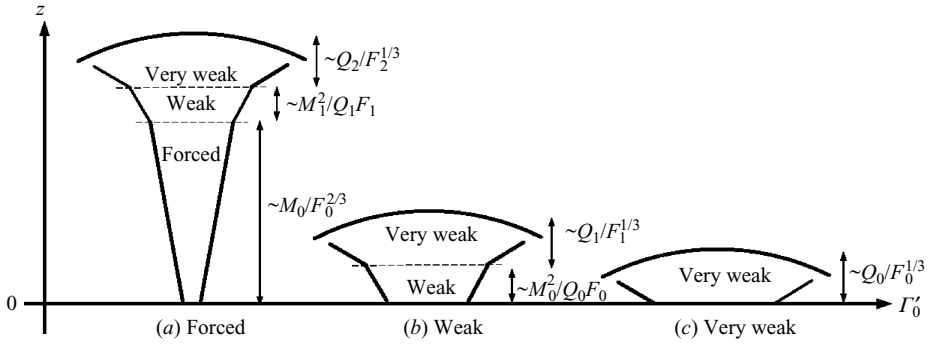

FIGURE 5. Summary of rise height scalings.

We may express (2.18) in terms of Γ_0' as

$$\zeta_{ss} = \frac{3}{2^{2/3}c_d^{2/3}}\alpha_{jet}^{2/3}\Gamma_0'^{-1/3} \approx 0.26\Gamma_0'^{-1/3}, \tag{2.19}$$

assuming $c_d = 1$ and $\alpha_{jet} = 0.0515$.

3. Discussion and conclusions

Following a method proposed by Kaye & Hunt (2006) for axisymmetric fountains we have expressed the conservation equations for a turbulent line fountain in terms of the local Richardson number Γ_l' and fountain width β. The equations were solved for the initial (maximum) rise height and three classes of fountain behaviour have been identified – forced, weak and very weak. Figure 4 shows the initial rise height plotted against the source Froude number ($Fr_0 \sim \Gamma_0'^{-1/2}$) covering all three regimes and summarizes the scalings expected in each. Also shown are the published experimental results (○) and the numerical results for the steady rise height of Lin & Armfield (2000) (□). Generally good comparisons are seen, especially when considering the innate difficulties in producing controlled line fountains with constant fluxes per unit length under laboratory conditions (particulary for small source Froude numbers).

The rise height scalings for forced ($z_m \sim M_0/F_0^{2/3}$, from (2.13)), weak ($z_m \sim M_0^2/Q_0F_0$, from (2.16)) and very weak fountains ($z_m \sim Q_0/F_0^{1/3}$, from (2.19)) are summarized in figure 5. For the highly forced fountain source we expect transition to weak fountain behaviour for $\Gamma_l'(\zeta) \approx 1$. The length scale for this fraction of the total rise height is $\sim M_0/F_0^{2/3}$ and is governed by the source momentum and buoyancy fluxes. The subsequent vertical extent $\sim M_1^2/Q_1F_1$ of the weak component of the fountain depends on the local fluxes of momentum, volume and buoyancy at the height of transition (the subscript 1 denoting values at the first transition). The final component of the total rise is the very weak fountain regime of extent $\sim Q_2/F_2^{1/3}$ (the subscript 2 denoting values at the second transition). Whilst this length scale was deduced by considering fluid spilling over the edge of a nozzle in the near field (figure 3*b*), in the far field of a highly forced fountain source (figure 5*a*), where the momentum flux is sufficiently weak, $Q_2/F_2^{1/3}$ is also expected to provide the characteristic length scale. It is apparent then that the maximum rise height predicted in the literature for a highly forced source and expressed as a multiple of the jet length ($M_0/F_0^{2/3}$) agrees well with measurements as $M_0/F_0^{2/3} \gg \{M_1^2/Q_1F_1, Q_2/F_2^{1/3}\}$. This is evident from figure 6 which shows the fountain regime based on our classification as a function of Γ_0' and

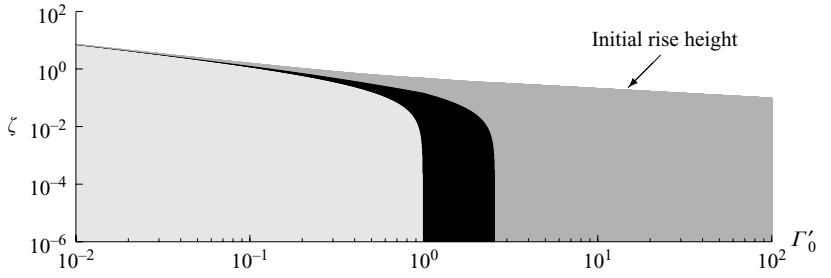

FIGURE 6. The fountain regime as a function of Γ_0' and height above the source. The light grey region highlights where the fountain is forced, the black region where the fountain is weak and the dark grey region where the fountain is very weak.

height above the source. The light grey highlights the vertical extent over which the fountain is forced, the black highlights where the fountain is weak and the dark grey highlights where it is very weak. It is clear that, for fountains issuing from highly forced sources, the forced regime is maintained over the vast majority of the entire rise height. This suggests $\alpha = \alpha_{jet}$ is the appropriate entrainment coefficient over the range of forced source conditions. Within both the black and grey regions our weak and very weak fountain models predict rise heights independent of the choice of α. Also clear from figure 6 is the limited region that the weak fountain regime occupies in the $\{\Gamma_0', \zeta\}$ parameter space despite this region being the focus of many of the experimental studies.

The analysis and classification presented has focused on fountains whose development is independent of the source Reynolds number Re_0. Williamson *et al.* (2008) have shown that $Re_0 > 2000$ is required to ensure fully turbulent flow in axisymmetric fountains from circular sources. For $Re_0 < 120$ the flow pattern observed varies strongly with the source Reynolds number resulting in a departure from the large Re_0 scalings for rise height. It would be informative if a similar study was performed for line fountains and our classification extended to low Re_0 flows.

By bringing together all the available data on high-Reynolds-number line fountain rise heights and comparing with the scalings derived from plume theory and from a description of fluid spilling over a boundary, we have been able to predict the fountain rise height over the complete range of source Froude number. The change in the fountain behaviour with height deduced and in the characteristic length scales over which these behaviours occur reveals a complex pattern of flow within the fountain. We anticipate that this insight will assist in the development of improved models for fountains.

REFERENCES

BAINES, W. D., TURNER, J. S. & CAMPBELL, I. H. 1990 Turbulent fountains in an open chamber. *J. Fluid Mech.* **212**, 557–592.

BATCHELOR, G. K. 1967 *An Introduction to Fluid Mechanics*. Cambridge University Press. ISBN 0–512–66396–2.

BLOOMFIELD, L. J. & KERR, R. C. 1998 Turbulent fountains in a stratified fluid. *J. Fluid Mech.* **358**, 335–356.

CAMPBELL, I. H. & TURNER, J. S. 1989 Fountains in magma chambers. *J. Petrol.* **30** (4), 885–923.

COOPER, L. Y. 1988 Ceiling jet-driven wall flows in compartment fires. *Combust. Sci. Tech.* **62**, 285–296.

Guyonnaud, L., Solliec, C., de Virel, M. D. & Rey, C. 2000 Design of air curtains used for area confinement in tunnels. *Exp. Fluids* **28**, 377–384.

Hunt, G. R. & Kaye, N. G. 2001 Virtual origin correction for lazy turbulent plumes. *J. Fluid Mech.* **435**, 377–396.

Kaye, N. B. & Hunt, G. R. 2006 Weak fountains. *J. Fluid Mech.* **558**, 319–328.

Kaye, N. B. & Hunt, G. R. 2007 Overturning in a filling box. *J. Fluid Mech.* **576**, 297–323.

Kerr, R. A. & Turner, J. S. 2008 *Personal communication.*

Kotsovinos, N. E. & List, E. J. 1977 Plane turbulent buoyant jets. Part 1. Integral properties. *J. Fluid Mech.* **81**, 25–44.

Lin, W. & Armfield, S. W. 2000 Very weak fountains in a homogeneous fluid. *Num. Heat Transfer Part* A **38**, 377–396.

Liu, Q. A. & Linden, P. F. 2006 The fluid dynamics of an underfloor air distribution system. *J. Fluid Mech.* **554**, 323–341.

Morton, B. R., Taylor, G. I. & Turner, J. S. 1956 Turbulent gravitational convection from maintained and instantaneous sources. *Proc. Roy. Soc. Lond.* A **234**, 1–23.

Turner, J. S. 1966 Jets and plumes with negative or reversing buoyancy. *J. Fluid Mech.* **26**, 779–792.

White, F. M. 2003 *Fluid Mechanics*, fifth edn. McGraw-Hill.

Williamson, N., Srinarayana, N., Armfield, S. W., Mcbain, G. D. & Lin, W. 2008 Low-Reynolds-number fountain behaviour. *J. Fluid Mech.* **608**, 297–317.

Zhang, H. & Baddour, R. E. 1997 Maximum vertical penetration of plane turbulent negatively buoyant jets. *J. Engng Mech.* **123** (10), 973–977.